



Numerical methods for the Poisson–Fermi equation in electrolytes



Jinn-Liang Liu

Department of Applied Mathematics, National Hsinchu University of Education, Hsinchu 300, Taiwan

ARTICLE INFO

Article history:

Received 31 December 2012

Received in revised form 18 March 2013

Accepted 27 March 2013

Available online 10 April 2013

Keywords:

Poisson–Boltzmann and Poisson–Fermi equations

Electrolyte

Ion channel

Correlation and steric effects

Numerical methods

ABSTRACT

The Poisson–Fermi equation proposed by Bazant, Storey, and Kornyshev [Phys. Rev. Lett. 106 (2011) 046102] for ionic liquids is applied to and numerically studied for electrolytes and biological ion channels in three-dimensional space. This is a fourth-order nonlinear PDE that deals with both steric and correlation effects of all ions and solvent molecules involved in a model system. The Fermi distribution follows from classical lattice models of configurational entropy of finite size ions and solvent molecules and hence prevents the long and outstanding problem of unphysical divergence predicted by the Gouy–Chapman model at large potentials due to the Boltzmann distribution of point charges. The equation reduces to Poisson–Boltzmann if the correlation length vanishes. A simplified matched interface and boundary method exhibiting optimal convergence is first developed for this equation by using a gramicidin A channel model that illustrates challenging issues associated with the geometric singularities of molecular surfaces of channel proteins in realistic 3D simulations. Various numerical methods then follow to tackle a range of numerical problems concerning the fourth-order term, nonlinearity, stability, efficiency, and effectiveness. The most significant feature of the Poisson–Fermi equation, namely, its inclusion of steric and correlation effects, is demonstrated by showing good agreement with Monte Carlo simulation data for a charged wall model and an L type calcium channel model.

© 2013 Elsevier Inc. All rights reserved.

1. Introduction

For more than 100 years since the seminal works of Gouy [1] and Chapman [2] on dilute solution theory, a great deal of effort has been devoted to improving the Poisson–Boltzmann (PB) theory of continuum models for a proper description of steric and correlation effects in electrolytes and ionic liquids [3–30]. For a partial list of review papers on this subject, we refer to [31–41] and references therein. In particular, Bazant et. al. give a comprehensive account of historical developments concerning these effects in [40]. Based on Santangelo's work [23], Bazant, Storey, and Kornyshev recently propose in [29] a novel PB modification called the Poisson–Fermi (PF) equation in which both steric and correlation effects are included to study the crowding and overscreening properties of ionic liquids in the double layer at large voltages. The results predicted by this new model are consistent with those of molecular dynamic simulations and experiments.

The Poisson–Fermi equation is a fourth-order nonlinear PDE, where the fourth-order term describes the medium permittivity and the dielectric response of correlated ions. Steric effects are seen in the resulting Fermi-like distribution of finite size ions at large potentials near electrodes and boundaries. The Fermi distribution is a consequence of classical lattice models used in [12,38,42] to describe the configurational entropy of electrolytes and avoids the long and outstanding problem of unphysical divergence predicted by the Gouy–Chapman model at large potentials due to the Boltzmann distribution of point

E-mail address: jinnliu@mail.nhcue.edu.tw

charges. The fourth-order term with respect to the potential function resembles a surface energy of Cahn–Hilliard type [43] that describes the phase transition of a binary fluid in interfacial region.

Apart from the PF approach, the density functional (continuum) description of ion–ion, ion–solute, or ion–water Lennard–Jones interactions has been independently proposed and intensively studied by Eisenberg’s group [26,44–46], called the EnVarA (energy variational analysis) approach herein, and by Wei’s group [30,47], called VMM (variational multiscale models) approach, in recent years to deal with steric and correlation effects. The layering of charged wall model and the binding of calcium to DEEA and EEEE channels have been observed by the EnVarA approach in one dimensional setting. In addition to describe these effects, the VMM approach can also generate molecular surfaces that are free of geometric singularities and are shown to be quite similar to that obtained by the MSMS package [48]. Moreover, the surface function satisfying the Laplace–Beltrami equation in VMM can be used to define a dielectric function that varies from the molecular domain to the solvent domain within the phase transition region. This is a differential geometric method whereas the PF approach uses a physical decomposition of the Coulomb interaction into short, intermediate, and long range components parametrized by the correlation length to define the dielectric function. It is shown in [49] by Monte Carlo (MC) simulations that the ionic selectivity of calcium channels is strongly affected by the dielectric properties within the channel pore region. It is however remained to be investigated whether these three continuum approaches can reproduce MC results in this respect. One of the main results in this paper is to compare PF and MC results on the charge distribution of electrolytes near a highly charged surface. The EnVarA and VMM approaches should produce Fermi-like distribution due to the L–J repulsion effects. The nonlinear Poisson equation proposed in [50] offers another way to treat intensive charges that give rise to hyperpolarization effects in proteins. Nevertheless, it is unknown to the author that there are comparison results of EnVarA or VMM to MC on charged wall models in three dimensional setting as shown in the present work. A final point to make is the dissipation principle [51–55] of ionic flows in solvent water, which forms the basis of the EnVarA approach. Since the dissipative force acting on an ionic species is customarily expressed in terms of its electrochemical potential and velocities of ions and solvent molecules, the electrostatic potential obtained via the PF approach can be straightforwardly used in the EnVarA models or equivalently the mixing entropy and correlation terms in the PF energy functional can be included in the EnVarA variational functional. This combination may provide opportunities to improve the Poisson–Nernst–Planck theory on its prediction or description of a range of fluid properties such as conductance [56–59], dielectric boundary force [60–69], diffusion distribution [61,70], and osmotic pressure [71].

We propose here a generalization of the Fermi distribution involving all ions up to four species and solvent molecules for biological ion channel modeling and a simple method to deal with the fourth-order term by reducing the PF equation to two second-order PDEs. Suitable boundary conditions then follow from Gauss’s divergence theorem and the global charge neutrality condition for these equations. The jump conditions across the molecular surface are extended from those of PB equation. The four species ions, sodium Na^+ , potassium K^+ , calcium Ca^{2+} , and chloride Cl^- , make the plasma needed to sustain the life of cells and proteins and are called “bio-ions” by Eisenberg because of their biological importance [41,72–74].

One of the difficulties in modeling biological systems by implicit solvent models is that their numerical approximation can be drastically hurt by geometric singularities of molecular surfaces that separate solvent domain from biomolecular domain. For the PB equation, this issue has been intensively studied in [75], where a second-order finite difference method called the matched interface and boundary (MIB) method is developed. The method is simplified (SMIB) here by assuming that each interface position is located at the middle of its two neighboring grid points. This is not a severe limitation for the overall approximation of a model system since the molecular surface itself is an artifact [76] and its generation by using the rolling-ball algorithm [77] or MSMS [48] is also error-prone. Moreover, the interface of a protein and an ionic solution depends dynamically on a wide range of conditions, for example, polarizability and flexibility of the protein, concentration, valence, and size of ions, and spatial distribution of polarization and number density of solvent molecules. It is therefore more adequate to make the protein wall soft enough or less restrictive [70] than to fix its position at rigid location by any surface generation scheme. Molecular surfaces defined by the SMIB method are also free of geometric singularities. The SMIB method is much easier to implement in 3D and basically gives the same optimal order of convergence as the original one. The approximation of continuum models in 3D is essential if correlations produced by ion crowding are to be dealt with. Biological functions of channel proteins depend sensitively on the complex structure of the channel containing ions. These can only be described in three dimensions [41,72–74]. Crowding near electrodes may be somewhat less sensitive to the dimensionality of the model, but a correct low dimensional ‘reduced mode’ can only be evaluated by comparison with a full three dimensional model and calculation [26,41,72].

Nonlinearity is another issue in practice. Physical phenomena such as phase transition in the electric double layer structure near charged surfaces, rapid and large variation of ionic concentrations from bath to channel narrow pore, high charge density in side chains, singular atomic charges in protein, and dielectric response of solvent molecules etc. are in general strongly nonlinear. Consequently, stable and fast convergence of nonlinear iterative methods inherited from the nonlinear model system is notoriously difficult to acquire in realistic simulations [70,78,79]. The PF equation is highly nonlinear in the sense that the fourth-order term describes not only the gradient but also the curvature of charge density profiles and that the steric effect is expressed as a nonlinear functional of electrostatic potential and the total bulk fraction of ions, which is very sensitive to the size of ions. A continuation method [80] is developed here to resolve these problems by introducing two continuation parameters into the steric and correlation terms, respectively. An algorithm for solving PB and PF equations iteratively is then presented.

Four model examples, namely, the gramicidin A (GA) channel model in [79], the Born ion model in [75], the charged wall model in [45,81], and the EEEE calcium channel model in [82], are studied by the PB or PF equation. Numerical results have shown that the SMIB method is optimal and accurate and that PB or PF results are in good accord with those of MC. An improvement of the PB equation on steric and correlation effects by the PF equation is thus demonstrated here for electrolytic and ion channel modeling.

The remaining part of the paper is organized as follows. The PF equation is presented in Section 2 with the new formulation of its reduced second-order system. Numerical methods for the PB and PF equations are gathered in Section 3. Section 4 provides all numerical results performed in this study. Some concluding remarks are given in Section 5.

2. The Poisson–Fermi equation

Using classical entropy models and the Cahn–Hilliard type of interfacial surface energy, the Landau–Ginzburg-like free energy functional

$$G = \int_{\Omega} d\mathbf{r} \frac{k_B T}{\bar{v}} \left\{ \sum_i \bar{v} C_i \ln(\bar{v} C_i) + \left(1 - \bar{v} \sum_i C_i \right) \ln \left(1 - \bar{v} \sum_i C_i \right) \right\} + \int_{\Omega} d\mathbf{r} \left\{ \frac{-\epsilon}{2} \left[|\nabla \phi|^2 + l_c (\nabla^2 \phi)^2 \right] + \phi \left(\sum_i q_i C_i + \sum_j q_j \delta_j \right) \right\} + \oint_{\partial\Omega_{\sigma}} d\mathbf{s} \sigma \phi \quad (2.1)$$

proposed in [29] is applied here to biological ion channel modeling, where C_i is the concentration of an ion species i carrying charge $q_i = ez_i$ with the unit charge e and the valence z_i , ϕ is the electrostatic potential, k_B is the Boltzmann constant, T is the absolute temperature, ϵ is the electric permittivity, l_c is an electrostatic correlation length, $\delta_j = \delta(\mathbf{r} - \mathbf{r}_j)$ is the delta function denoting a fixed atomic charge q_j located at \mathbf{r}_j , and σ is the surface charge density on a surface area $\partial\Omega_{\sigma} \subset \partial\Omega$ the boundary of a bounded domain $\Omega \subset \mathbf{R}^3$, if any. The entropy expressed by the first integral involves all ions and solvent molecules by means of the total volume fraction defined as $v = \sum_i d_i^3 C_i^{\text{Bulk}} = \bar{v} \sum_i |z_i| C_i^{\text{Bulk}}$, where d_i are diameters of ions and C_i^{Bulk} are bulk concentrations. The correlation term in the second integral accounts for the dielectric response of the electrolyte.

In equilibrium, the variation of the functional with respect to ϕ and C_i yields the Poisson–Fermi equation

$$\epsilon \left(l_c^2 \nabla^2 - 1 \right) \nabla^2 \phi(\mathbf{r}) = \sum_i q_i C_i(\mathbf{r}) + \sum_j q_j \delta(\mathbf{r} - \mathbf{r}_j) = \rho(\mathbf{r}) \quad (2.2)$$

with

$$C_i(\mathbf{r}) = C_i^{\text{Bulk}} \exp(-\beta_i \phi - S) \quad (2.3)$$

$$S = \ln \left(1 - v + v(z_- \exp(-\beta_+ \phi) + z_+ \exp(-\beta_- \phi)) / (z_+ + z_-) \right), \quad (2.4)$$

where $\beta_i = z_i e / (k_B T)$ and S is called here a steric functional with z_+ and z_- being the sums of absolute values of valences of cations and anions, respectively (β_{\pm} are similarly defined). For example, $z_+ = 2$ and $z_- = 1$ for a 2:1 electrolyte [81] and $z_+ = 1 + 2$ and $z_- = 1 + \frac{1}{2}$ for the EEEE calcium channel model in [82] that involves four species of ions, i.e., $C_1 = C_{\text{Na}^+}$, $C_2 = C_{\text{Ca}^{2+}}$, $C_3 = C_{\text{Cl}^-}$, and $C_4 = C_{\text{O}^{1/2-}}$, where the glutamate (E) is expressed by a structural oxygen ion $\text{O}^{1/2-}$. Moreover, for the 2:1 electrolyte, we have

$$C_1 = \frac{1}{d_1^3} \frac{1}{1 + 3(1 - v) \exp(\beta_1 \phi) / v} \quad (2.5)$$

that resembles the Fermi–Dirac distribution in which the excluded volume interaction plays the role of the Pauli principle [29]. For large negative potentials $-\beta_1 \phi \gg 1$, the concentration is saturated to $C_1^{\text{Max}} = 1/d_1^3$. Without the steric functional S , the distribution is of Boltzmann that would result in absurdly large concentration of counterions near a highly charged surface even for a very dilute electrolyte [17]. From this model, the dielectric function $\hat{\epsilon} = \epsilon(1 - l_c^2 \nabla^2)$, whose Fourier transform $\hat{\epsilon}_k = \epsilon(1 + l_c^2 k^2)$ is valid for wave number $|k| \ll l_c^{-1}$, approximates the medium permittivity and the linear response of correlated ions [29]. Moreover, this model provides not only the gradient of charge density $\rho = -\epsilon \nabla^2 \phi$ (third order derivative from the perspective of the PB equation) but also the curvature of the density (fourth order derivative). These physical properties, generally inexplicable by the standard PB equation, can be used to study sensitive phenomena such as the interplay between overscreening from short-range correlations and crowding from finite size effects at large potentials [29,40].

The central finite difference approximation of the PF equation leads to a matrix system in which the maximum number of nonzero entries in each row of the sparse matrix, called the compressed bandwidth of the matrix hereafter, is 19 due to the fourth order derivative term. In practice, sparse square matrices are usually compressed to rectangular matrices, where the total number of columns is equal to the compressed bandwidth. The memory demand for (2.2) is thus nearly triple that of second-order PDEs for which the corresponding compressed bandwidth is 7. In fact, the most challenging part in discretization will be the numerical treatment of high order (up to the third order) derivatives across the molecular surface

Γ between the solvent Ω_s and biomolecular Ω_m regions of a channel model, i.e., $\Gamma = \bar{\Omega}_s \cap \bar{\Omega}_m$ and $\bar{\Omega} = \bar{\Omega}_s \cup \bar{\Omega}_m$, where the dielectric constant ϵ_r in $\epsilon = \epsilon_r \epsilon_0$ is discontinuous and the geometric property is highly irregular or even singular [75,76].

To bypass these potential difficulties, we propose a simple approach to deal with this fourth-order problem by reducing (2.2) to two second-order PDEs

$$\epsilon \left(l_c^2 \nabla^2 - 1 \right) \Psi = \rho, \quad \nabla^2 \phi = \Psi. \tag{2.6}$$

From these two equations and Gauss’s divergence theorem, the global charge neutrality condition implies that

$$\begin{aligned} 0 &= \int_{\partial\Omega_\sigma} \sigma ds + \int_{\Omega} \rho d\mathbf{r} = \int_{\partial\Omega_\sigma} \sigma ds + \int_{\Omega} \epsilon \left(l_c^2 \nabla^2 - 1 \right) \Psi d\mathbf{r} = \int_{\partial\Omega_\sigma} \sigma ds - \int_{\partial\Omega} \epsilon l_c^2 \nabla \Psi \cdot \mathbf{n} ds - \int_{\Omega} \epsilon \Psi d\mathbf{r} \\ &= \int_{\partial\Omega_\sigma} \sigma ds - \int_{\partial\Omega} \epsilon l_c^2 \nabla \Psi \cdot \mathbf{n} ds + \int_{\partial\Omega} \epsilon \nabla \phi \cdot \mathbf{n} ds, \end{aligned} \tag{2.7}$$

where \mathbf{n} is an outward normal unit vector on $\partial\Omega$. Consequently, we require the following boundary conditions for the reduced model (2.6)

$$\begin{aligned} -\epsilon \nabla \phi \cdot \mathbf{n} &= \sigma \text{ on } \partial\Omega_\sigma, \\ \nabla \phi \cdot \mathbf{n} &= 0 \text{ on } \partial\Omega \setminus \partial\Omega_\sigma, \\ \nabla \Psi \cdot \mathbf{n} &= 0 \text{ on } \partial\Omega. \end{aligned} \tag{2.8}$$

Note that the Neumann boundary condition is replaced by a Dirichlet one if the potential is specified on $\partial\Omega_\sigma$. The jump conditions across the interface Γ are

$$[\phi] = [\epsilon \nabla \phi \cdot \mathbf{n}] = [\Psi] = [\nabla \Psi \cdot \mathbf{n}] = 0, \tag{2.9}$$

where the jump function $[u]$ is defined as $[u] = u_m(\gamma) - u_s(\gamma)$ for all $\gamma \in \Gamma$ with $u_m(\gamma) = \lim_{\mathbf{r} \rightarrow \gamma} u(\mathbf{r})$ for $\mathbf{r} \in \Omega_m$ and $u_s(\gamma) = \lim_{\mathbf{r} \rightarrow \gamma} u(\mathbf{r})$ for $\mathbf{r} \in \Omega_s$.

The decomposition method in [83] is used to cope with the singular charges in (2.2), namely, the potential $\phi(\mathbf{r})$ is split as

$$\phi(\mathbf{r}) = \tilde{\phi}(\mathbf{r}) + \bar{\phi}(\mathbf{r}), \quad \mathbf{r} \in \bar{\Omega} \tag{2.10}$$

such that

$$\bar{\phi}(\mathbf{r}) = \begin{cases} \phi^*(\mathbf{r}) + \phi^0(\mathbf{r}), & \mathbf{r} \in \bar{\Omega}_m \\ 0, & \mathbf{r} \in \bar{\Omega}_s \setminus \Gamma \end{cases}, \quad \tilde{\phi}(\mathbf{r}) = \begin{cases} \phi - \phi^* - \phi^0, & \mathbf{r} \in \bar{\Omega}_m \\ \phi, & \mathbf{r} \in \bar{\Omega}_s \setminus \Gamma \end{cases}. \tag{2.11}$$

The PB equation is then decomposed to

$$\begin{aligned} -\nabla \cdot \left(\epsilon \nabla \tilde{\phi}(\mathbf{r}) \right) &= \sum_{i=1}^2 q_i C_i(\mathbf{r}), \quad \mathbf{r} \in \Omega \setminus \Gamma, \tag{2.12} \\ -\Delta \phi^0(\mathbf{r}) &= 0, \quad \mathbf{r} \in \Omega_m, \quad \phi^0(\mathbf{r}) = \phi^*(\mathbf{r}), \quad \mathbf{r} \in \partial\Omega_m, \tag{2.13} \end{aligned}$$

with ϕ^* being the Green function given analytically

$$\phi^*(\mathbf{r}) = \sum_j \frac{q_j}{4\pi\epsilon_m\epsilon_0 |\mathbf{r} - \mathbf{r}_j|}, \quad \mathbf{r} \in R^3. \tag{2.14}$$

The corresponding jump conditions are

$$[\phi] = [\epsilon \nabla \phi \cdot \mathbf{n}] = [\tilde{\phi}] = 0, \quad [\epsilon \nabla \tilde{\phi} \cdot \mathbf{n}] = -\epsilon_m \epsilon_0 \nabla (\phi^* + \phi^0) \cdot \mathbf{n}. \tag{2.15}$$

For calculating the potential ϕ , we need to solve (2.13) once for all and then solve (2.12) by Newton’s method.

3. Numerical methods

The central finite difference (FD) approximation of the Poisson equation $-\nabla^2 \phi = f$ in 3D at any grid point $\mathbf{r}_{ijk} = (x_i, y_j, z_k)$ is

$$\frac{-\phi_{i-1,j,k} + 2\phi_{ijk} - \phi_{i+1,j,k}}{\Delta x^2} + \frac{-\phi_{i,j-1,k} + 2\phi_{ijk} - \phi_{i,j+1,k}}{\Delta y^2} + \frac{-\phi_{i,j,k-1} + 2\phi_{ijk} - \phi_{i,j,k+1}}{\Delta z^2} = f_{ijk}, \tag{3.1}$$

where $\phi_{ijk} \approx \phi(x_i, y_j, z_k)$, $f_{ijk} = f(x_i, y_j, z_k)$, and Δx , Δy , and Δz are mesh sizes on the three axes. For simplicity, we use uniform partition, i.e., $\Delta x = \Delta y = \Delta z = h$. This leads to a sparse matrix system $A \vec{\phi} = \vec{f}$ with the compressed bandwidth of A being 7. The matrix size (i.e., the total number of grid points) is usually measured in millions for realistic 3D simulations. The

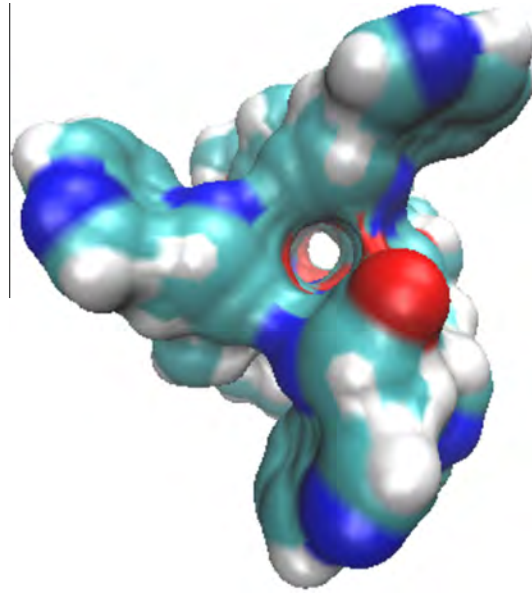


Fig. 1. Top view of GA channel.

compressed bandwidth of sparse matrices is hence a critical factor for the efficiency of Poisson solvers. The convergence order of this method is $O(h^2)$ (optimal) in maximum error norm for sufficiently smooth function ϕ . However, these efficient and effective properties can be easily degraded by geometric singularities of the interface Γ if they are not properly treated. For example, a second-order scheme is degraded to only of $O(h^{0.37})$ by this kind of singularities [84]. As noted in [75], molecular surfaces generated by well-known software such as MSMS [48] admit cusps and self-intersecting singularities. A top view of the GA channel surface generated by the VMD program [85] using MSMS is illustrated in Fig. 1 to show a typical simulation geometry of biological ion channels.

A 2D cross section of the GA channel embedded in a membrane is sketched in Fig. 2, where the biomolecular domain Ω_m is composed of the channel protein and the membrane and the solvent domain Ω_s consists of extracellular (upper), channel pore (central), and intracellular (lower) regions. The diameter of the channel pore in the narrowest part is about 4 Å making insufficient grid points for high order FD schemes to treat the jump conditions in (2.15). We simplify the matched interface and boundary method of [75] by using the standard 7-point FD scheme. For conciseness, the scheme is described for the 1D Poisson equation

$$-\frac{d}{dx} \left(\epsilon(x) \frac{d\phi(x)}{dx} \right) = f(x) \quad (3.2)$$

as the corresponding 3D case follows obviously in a similar way. For the jump conditions, we assume that every jump position $\gamma \in \Gamma$ is at the middle of its two neighboring grid points as shown in Fig. 3, i.e.,

$$x_{i-1} < \gamma = x_{i-\frac{1}{2}} < x_i. \quad (3.3)$$

The main idea of the MIB method is

- (1) considering (3.2) as two subproblems on two disjoint subdomains $x < \gamma$ and $x > \gamma$,
- (2) treating the jump conditions (2.15) as the boundary conditions of the subproblems,
- (3) extending smoothly a function $\phi(x)$ defined on a subdomain to a ‘fictitious’ function $\psi(x)$ defined on the other subdomain,
- (4) applying Taylor’s theorem to the jump conditions, and joining two subproblems back to one.

The resulting FD formulas across the jump position γ with the jumps $[\phi]$ and $[\epsilon\phi']$ are

$$\frac{-\epsilon_{i-\frac{3}{2}}\phi_{i-2} + \left(\epsilon_{i-\frac{3}{2}} + (1 - A_1)\epsilon_{i-\frac{1}{2}}^- \right)\phi_{i-1} - A_2\epsilon_{i-\frac{1}{2}}^-\phi_i}{\Delta x^2} = f_{i-1} + \frac{\epsilon_{i-\frac{1}{2}}^- A_0}{\Delta x^2} \quad (3.4)$$

$$\frac{-B_1\epsilon_{i-\frac{1}{2}}^+\phi_{i-1} + \left((1 - B_2)\epsilon_{i-\frac{1}{2}}^+ + \epsilon_{i+\frac{1}{2}} \right)\phi_i - \epsilon_{i+\frac{1}{2}}\phi_{i+1}}{\Delta x^2} = f_i + \frac{\epsilon_{i-\frac{1}{2}}^+ B_0}{\Delta x^2}, \quad (3.5)$$

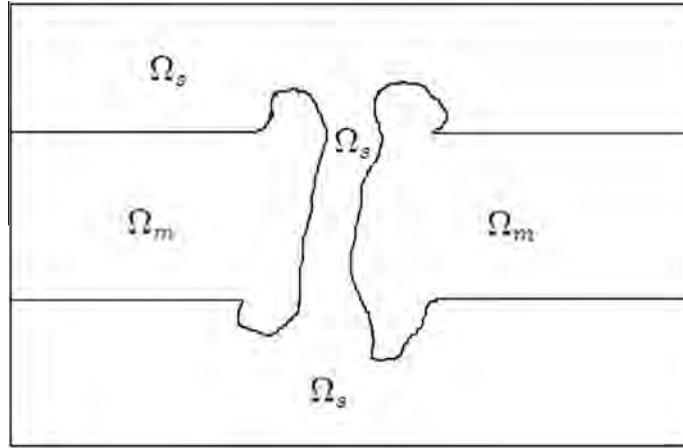


Fig. 2. A cross section of 3D PF simulation domain for GA channel.

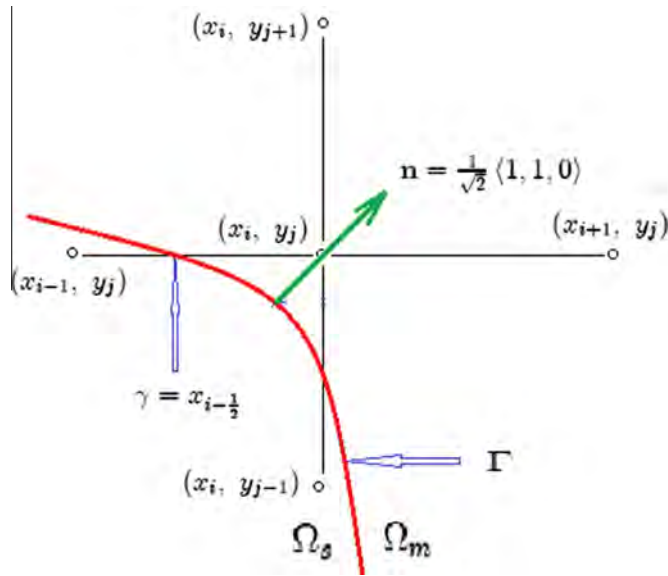


Fig. 3. Interface position γ .

where

$$A_1 = \frac{-(\epsilon_m - \epsilon_s)}{\epsilon_m + \epsilon_s}, \quad A_2 = \frac{2\epsilon_m}{\epsilon_m + \epsilon_s}, \quad A_0 = \frac{-2\epsilon_m[\phi] - \Delta\chi[\epsilon\phi']}{\epsilon_m + \epsilon_s} \quad (3.6)$$

$$B_1 = \frac{2\epsilon_s}{\epsilon_m + \epsilon_s}, \quad B_2 = \frac{\epsilon_m - \epsilon_s}{\epsilon_m + \epsilon_s}, \quad B_0 = \frac{2\epsilon_s[\phi] - \Delta\chi[\epsilon\phi']}{\epsilon_m + \epsilon_s}. \quad (3.7)$$

We now briefly describe Newton’s method for dealing with the nonlinearity of PB and PF equations. For PB equation, Gâteaux’s differentiation of

$$G(\phi) = -\nabla \cdot (\epsilon \nabla \phi) - \rho(\phi) = 0 \quad (3.8)$$

with respect to ϕ yields the linearized PB equation

$$-\nabla \cdot (\epsilon \nabla \phi_1) - \rho'(\phi_0)\phi_1 = \rho(\phi_0) - \rho'(\phi_0)\phi_0 \quad (3.9)$$

for which we seek the solution ϕ_1 with ϕ_0 being given and $\rho'(\phi_0)$ being the derivative of ρ at ϕ_0 . This linear equation can be iteratively solved by replacing the old function ϕ_0 by the newly found solution ϕ_1 and so on with initial potential $\phi_0 = 0$ and

initial bulk concentrations C_i^{Bulk} . Similarly, the Poisson–Fermi solution is calculated by iteratively solving the linearized equation

$$\epsilon \left(l_c^2 \nabla^2 - 1 \right) \nabla^2 \phi_1 - \rho'(\phi_0) \phi_1 = \rho(\phi_0) - \rho'(\phi_0) \phi_0. \tag{3.10}$$

Corresponding to (2.6), the linearized PF equations are

$$\nabla \cdot \epsilon l_c^2 \nabla \Psi_1 - \epsilon \Psi_1 = \rho(\phi_0), \quad \nabla^2 \phi_1 - \rho'(\phi_0) \phi_1 = \Psi_1 - \rho'(\phi_0) \phi_0, \tag{3.11}$$

which result in the following linear algebraic systems

$$B \vec{\Psi}_1 = \vec{\rho}_0, \quad A \vec{\phi}_1 + D \vec{\phi}_1 = \vec{\Psi}_1 + \vec{\phi}_0 \tag{3.12}$$

where the compressed bandwidth of A and B is 7 and D is a diagonal matrix.

In 3D, the steric functional (2.4) makes the algebraic systems highly unstable and sensitive to the accuracy of previous iterative solutions ϕ_0 , i.e., the nonlinear iteration can easily diverge or converge very slowly if no extra effort is made. To accelerate the convergence, we apply the continuation method [80] to the steric functional which is replaced by

$$\lambda_S S, \quad \lambda_S = 0 + k \Delta \lambda, \quad k = 0, 1, 2, \dots, \frac{1}{\Delta \lambda}, \tag{3.13}$$

where λ_S is the continuation parameter and its stepping length $\Delta \lambda$ can be determined adaptively in run-time or simply by trial and error. Hence, we get solutions without finite size effects when $\lambda_S = 0$ and with full size when $\lambda_S = 1$. Solutions of step k will be used as initial guesses for seeking solutions of the next step $k + 1$. The correlation length l_c in the fourth-order operator might also complicate the convergence property and hence should be multiplied by a similar continuation parameter λ_F .

We summarize the above numerical methods in the following algorithm.

1. Solve nonlinear PB $-\nabla \cdot (\epsilon \nabla \phi) = \rho(\phi)$ with the steric functional $S = 0$.
2. Solve nonlinear PB $-\nabla \cdot (\epsilon \nabla \phi) = \rho(\phi)$ with $\lambda_S S \neq 0$ and set $\phi_0 = \phi$.
3. Solve linear PF1 $-\nabla \cdot \epsilon (\lambda_F l_c)^2 \nabla \Psi + \epsilon \Psi = -\rho(\phi_0)$.
4. Solve linear PF2 $-\nabla^2 \phi + \rho'(\phi_0) \phi = -\Psi + \rho'(\phi_0) \phi_0$. Go to 3 until convergence.

The solution of any step will be used as an initial guess for the next step. The very first initial guesses are $\phi = 0$ for potential and $C_i = C_i^{\text{Bulk}}$ for concentrations. In Step 1, there is a loop of Newton’s iteration since the PB is nonlinear. Similarly, there is a Newton loop in Step 2 for each continuation parameter λ_S . The continuation loop thus embodies the Newton loop. The last loop in Steps 3 and 4 is a Newton loop, which is also contained in an outer continuation loop due to the continuation parameter λ_F .

It should be emphasized that the total number of iterations in Newton and continuation loops can be extremely large or even infinity from the biological point of view since both local potentials and transmembrane potentials are almost never small enough to guarantee that the sequence of approximate solutions generated by Newton’s method definitely lies within the convergence ball of the exact solution in the solution manifold [86]. In fact, most mathematical and numerical analyses of the PF equation concerning, for example, analytical solutions [87], existence and uniqueness [88], error estimates [89–91], and nonlinear solvers [78,80,92–95] remain to be investigated.

4. Numerical results

The Poisson, Poisson–Boltzmann, and Poisson–Fermi equations are applied to four model problems. First, the GA channel model in [79] is used to verify the optimal convergence of the SMIB method. Second, the Born ion model in [75] is used to validate the potential decomposition and SMIB methods. Third, the Poisson–Fermi equation is fully tested by two charged wall model problems in [45,81], where the Monte Carlo results are available for comparison. Fourth, an L type calcium channel model in [82] with MC data is used to verify the Poisson–Fermi equation.

Table 4.1
Errors in L_∞ norm.

h in Å	MIB		SMIB	
	Error	Order	Error	Order
2.00			0.4466	
1.00	0.1400		0.0922	2.28
0.50	0.0271	2.36	0.0228	2.02
0.25	0.0152	0.84	0.0057	2.00

Table 4.2
 ΔG .

h in Å	PBEQ	APBS	MIB	SMIB
1.000	–83.57	–83.44	–81.95	–82.06
0.500	–85.78	–85.85	–81.98	–81.98
0.250	–82.84	–82.58	–81.98	–81.98
0.125	–82.49	–82.27	–81.98	–81.98

Example 1. Defined on the realistic GA channel domain as illustrated in Figs. 1 and 2, where the enclosing box $\Omega = (-20 \text{ \AA}, 20 \text{ \AA}) \times (-20 \text{ \AA}, 20 \text{ \AA}) \times (-20 \text{ \AA}, 20 \text{ \AA})$, the Poisson equation is solved by the SMIB method with the exact solution $\phi(\mathbf{r}) = \cos x \cos y \cos z$ constructed in [79], $\epsilon_m = 1$, and $\epsilon_s = 80$. The atomic data of the channel protein is downloaded from the Protein Data Bank [96] with PDB ID: 1MAG [97]. The PDB2PQR software [98] is used to get partial charges and radii of the atoms. The molecular surface Γ of the channel is generated by rolling a probe ball (water molecule) with radius 1.4 Å over a total of 554 spherical atoms in the GA protein [77]. The membrane part as shown in Fig. 2 is taken as a uniform and continuous dielectric substrate without charges and is not processed by PDB2PQR. The optimal $O(h^2)$ convergence in the maximum error norm $L_\infty = \max_{ijk} |\phi(x_i, y_j, z_k) - \phi_{ijk}|$ is obtained by this method as shown in Table 4.1. The Poisson equation is linear and does not include singular or surface charges. Newton's method and the potential decomposition method are thus not needed for this example. Under the assumption (3.3), the molecular surface Γ is not fixed and is adaptively determined by the grid size h ranging from 2 Å to 0.25 Å. For $h = 0.25 \text{ \AA}$, the dimension of the matrix A in the linear system $A\vec{\phi} = \vec{f}$ is 4,096,000 for which it requires about 300 MB memory to store the compressed matrix system with double precision. It took about 2 min and 47 s on a laptop computer equipped with 1.3 GHz Intel CPU and 2 GB RAM to solve the linear system by the SOR method with the relaxation parameter being set to 1.9 and error tolerance set to 10^{-6} . The main purpose of this example is to show the simplicity and effectiveness of the SMIB method.

Compared with the MIB results [79] as duplicated in the table, the SMIB method is in general more accurate since it does not require any local transformation as that of Eq. (18) in [79] for handling the outward unit normal vector \mathbf{n} in (2.15) at interface points. The normal vector for the SMIB method is always defined as $\mathbf{n} = \langle 1/\sqrt{2}, 1/\sqrt{2}, 0 \rangle$, for example, if the molecular surface passes through any two neighboring points of $(x_i, y_j, 0)$ as shown in Fig. 3. Consequently, there are no geometric singularities such as kinks that would lead to ill-defined normal vectors under the assumption (3.3). On the other hand, the MIB method requires more technical schemes to deal with local partial derivatives associated with the transformation between the local coordinates and the actual coordinates since it uses the molecular surface generated by the above mentioned packages that often give very irregular interface points. The additional schemes certainly incur more errors in approximation and implementation. Of course, the SMIB and MIB methods are completely the same if all interface points for the MIB method satisfy the condition (3.3). They are different only in the way how the molecular surface is generated and utilized.

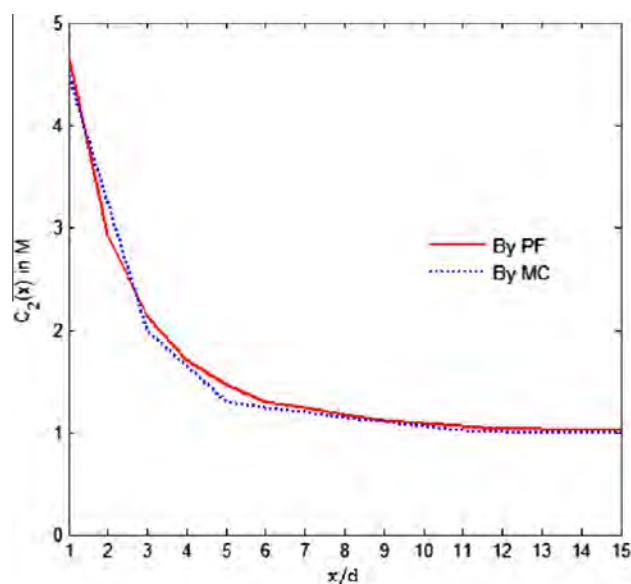


Fig. 4. C_2 concentration profiles obtained by PF and MC methods for a 1:1 electrolyte at 1 M with $\sigma = 0.1 \text{ C/m}^2$ and $d = 2 \text{ \AA}$.

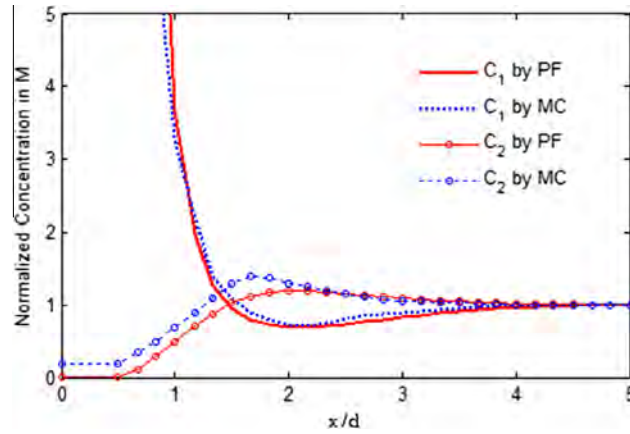


Fig. 5. Normalized [81] concentration profiles obtained by PF and MC methods for a 2:1 electrolyte at 1 M with $\sigma = -0.3 \text{ C/m}^2$ and $d = 3 \text{ \AA}$.

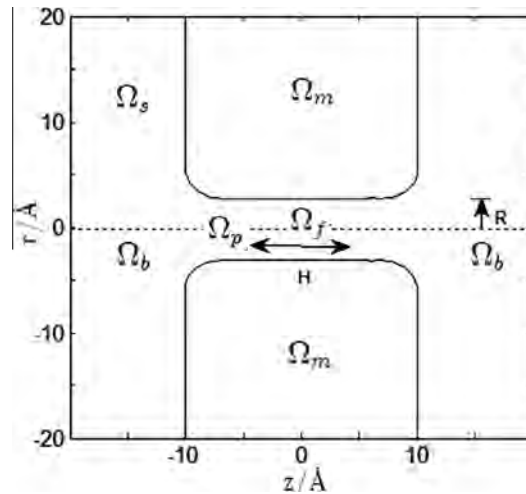


Fig. 6. A cross section of the cylindrical shaped channel model. The length and radius of the filter are H and R , respectively.

Example 2. The Born ion model is a classic example of a point charge in a spherical cavity of radius a solvated in water. With $a = 2 \text{ \AA}$, $\epsilon_m = 1$, $\epsilon_s = 80$, $q_j = q_1 = +e$, and $\mathbf{r}_1 = \mathbf{0}$ in (2.2), the solvation energy is given exactly as $\Delta G_{\text{Ex}} = -81.98 \text{ [kcal/mol]}$. This model can be described by the Poisson equation with a singular charge term. By the potential decomposition method (2.10), it is shown in [75] that the solvation energy can be approximated by $\Delta G = q_1 (\tilde{\phi}(\mathbf{0}) + \phi^0(\mathbf{0}))/2$. The interface of this model problem is $\Gamma = \partial\Omega_m = \{|\mathbf{r}| = a\}$, which is a sphere in $\Omega = (-20 \text{ \AA}, 20 \text{ \AA}) \times (-20 \text{ \AA}, 20 \text{ \AA}) \times (-20 \text{ \AA}, 20 \text{ \AA})$. In order to approximate the exact solvation energy more accurately, the assumption (3.3) should be modified according to the nonlinear extrapolation scheme in [75] for calculating the derivative of ϕ^0 in (2.15). The SMIB method essentially gives the same results as those by the original MIB method [75] as shown in Table 4.2 along with the results duplicated from [75] by the well-known software packages PBEQ [99] and APBS [100].

Example 3. We next consider electrolytes in the box $\Omega = (0 \text{ \AA}, 40 \text{ \AA}) \times (0 \text{ \AA}, 40 \text{ \AA}) \times (0 \text{ \AA}, 40 \text{ \AA})$ and a surface charge density σ being uniformly distributed on one wall (corresponding to the y -axis in Figs. 4 and 5) of the box. The boundary condition for the potential function ϕ is of Neumann type on the four walls adjacent to the charged wall and is of Dirichlet type on the opposite wall. For a 1:1 electrolyte with $\sigma = 0.1 \text{ C/m}^2$, $d = d_1 = d_2 = 2 \text{ \AA}$, and $\epsilon = 78.5$, the concentration profile of the negative ion species C_2 predicted by the PF equation with the correlation length $l_c = 0$ is in good agreement with MC results [45] as shown in Fig. 4. For another 2:1 electrolyte with $\sigma = -0.3 \text{ C/m}^2$ and $d_1 = d_2 = 3 \text{ \AA}$, a triple layer (Stern, diffuse, and overscreening layers) structure shown in Fig. 5 is captured by the PF equation with the correlation length $l_c = 0.6 \text{ \AA}$ and well matched to that of MC results presented in Fig. 4(a) in [81]. The overscreening layer, where the normalized concentration profile is below 1 M in Fig. 5, is unattainable by the standard PB equation even with the steric functional in our experience. The correlation length l_c is the only tuning parameter to fit MC data with the mesh size $h = 0.5 \text{ \AA}$.

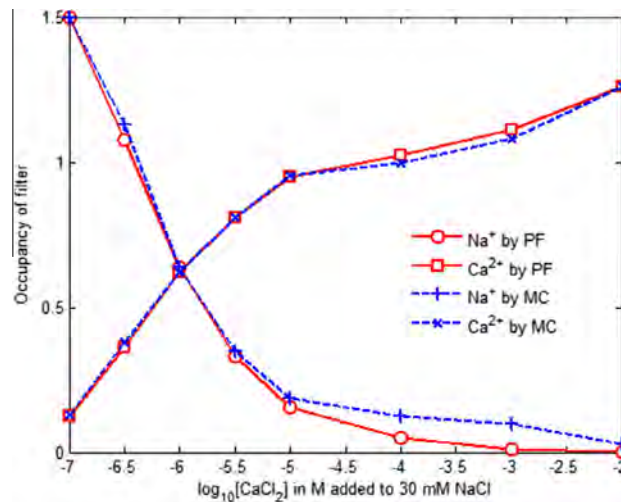


Fig. 7. The average number of Ca^{2+} and Na^+ in the selectivity filter calculated by PF and MC.

Example 4. The EEEE calcium channel geometry in [82] is depicted in Fig. 6 that shows a cross section of the cylindrical channel. The channel is placed in the central part of the domain box Ω as shown, where the solvent domain Ω_s consists of the channel pore and two baths and the molecular domain Ω_m consists of the channel protein and the membrane. The solvent domain is further partitioned into the filter region Ω_f , the channel pore region Ω_p , and the bath region Ω_b such that $\overline{\Omega_s} = \overline{\Omega_p} \cup \overline{\Omega_b}$, $\Omega_p \cap \Omega_b = \emptyset$, and $\Omega_f \subset \Omega_p$. The lengths of the filter and channel pore are $H = 10 \text{ \AA}$ and $L = 20 \text{ \AA}$, respectively, as considered in [82]. The radius of the pore is $R = 3.5 \text{ \AA}$.

All parameter values in [82] are used here, i.e., $d_1 = d_{\text{Na}^+} = 1.9 \text{ \AA}$, $d_2 = d_{\text{Ca}^{2+}} = 1.98$, $d_3 = d_{\text{Cl}^-} = 3.62$, $d_4 = d_{\text{O}^{1/2-}} = 2.8$, $\epsilon_s = 80$, and $\epsilon_m = 10$. The occupancy of Ca^{2+} and Na^+ calculated by PF with the correlation length $l_c = 0.577 \text{ \AA}$ and by MC is shown in Fig. 7, where the MC data is taken from [82]. The results of PF are again in good accord with those of MC. More detailed analysis, method description, and results for this problem by PF will be reported elsewhere.

5. Conclusions

The literature on the Poisson–Boltzmann equation and its modifications is enormous for its simple, elegant, and yet often inadequate description of electrostatic interactions in a variety of physical, chemical, and biological systems. The Poisson–Fermi equation is an analytical modification with both steric and correlation effects being taken into account. It has been shown to match molecular dynamic simulation results in ionic liquids and is shown in this paper to do well with Monte Carlo simulation results in electrolytes. This fourth-order PDE is reformulated here to two second-order PDEs to which the standard finite difference approximation is hence more feasible and manageable for handling geometric singularities of molecular surfaces in 3D implementation. Numerical results obtained by a simplified matched interface and boundary method presented here for treating these singularities confirm the theoretical and optimal convergence. Newton’s method and the continuation method are used to handle the nonlinear problems associated with the steric and correlation terms. Four model examples are extensively tested by the Poisson–Boltzmann and Poisson–Fermi solvers developed in this paper. Numerical evidence has been provided to attest the numerical methods and the novelty of the Poisson–Fermi equation.

Acknowledgement

This work was supported by National Science Council of Taiwan under Grant 99-2115-M-134-004-MY3. The author would like to express his gratitude to Bob Eisenberg and Dezsó Boda for their kind sharing and motivating discussions on channel modeling and to the reviewers for many valuable comments and suggestions on the manuscript.

References

- [1] M. Gouy, Sur la constitution de la charge électrique à la surface d’un électrolyte, *J. Phys.* 9 (1910) 457–468.
- [2] D.L. Chapman, A contribution to the theory of electrocapillarity, *Philos. Mag.* 25 (1913) 475–481.
- [3] N. Bjerrum, Die Dissoziation der starken Elektrolyte, *Zeitschr. f. Elektrochemie* 24 (1918) 321–328.
- [4] M. Born, Volumen und hydrations-swarme der ionen, *Z. Phys.* 1 (1920) 45–48.
- [5] P. Debye, E. Hückel, Zur Theorie der Elektrolyte. I. Gefrierpunktserniedrigung und verwandte Erscheinungen, *Phys. Zeitschr.* 24 (1923) 185–206.
- [6] O. Stern, Zur theorie der elektrolytischen doppelschicht, *Z. Elektrochem.* 30 (1924) 508–516.
- [7] L. Onsager, Electric moments of molecules in liquids, *J. Am. Chem. Soc.* 58 (1936) 1486–1493.
- [8] J.G. Kirkwood, The dielectric polarization of polar liquids, *J. Chem. Phys.* 7 (1939) 911–919.

- [9] J.J. Bikerman, Structure and capacity of electrical double layer, *Philos. Mag.* 33 (1942) 384–397.
- [10] T.B. Grimley, N.F. Mott, The contact between a solid and a liquid electrolyte, *Discuss. Faraday Soc.* 1 (1947) 3–11.
- [11] D.C. Grahame, Effects of dielectric saturation upon the diffuse double layer and the free energy of hydration of ions, *J. Chem. Phys.* 18 (1950) 903–909.
- [12] M. Dutta, S.N. Bagchi, On the distribution of ions in solutions of strong electrolytes, *Ind. J. Phys.* 24 (1950) 61.
- [13] V. Freise, Zur theorie der diffusen doppelschicht, *Zeitschr. f. Elektrochemie* 56 (1952) 822–827.
- [14] M. Eigen, E. Wicke, The thermodynamics of electrolytes at higher concentration, *J. Phys. Chem.* 58 (1954) 702–714.
- [15] R. Kjellander, S. Marčelja, Correlation and image charge effects in electric double layers, *Chem. Phys. Lett.* 112 (1984) 49–53.
- [16] A. Iglic, V. Kralj-Iglic, Influence of finite size of ions on electrostatic properties of electric double layer, *Electrotechnical Rev. (Slovenia)* 61 (1994) 127–133.
- [17] I. Borukhov, D. Andelman, H. Orland, Steric effects in electrolytes: a modified Poisson–Boltzmann equation, *Phys. Rev. Lett.* 79 (1997) 435–438.
- [18] S. Marčelja, Exact description of aqueous electrical double layers, *Langmuir* 16 (2000) 6081–6083.
- [19] J. Cervera, J.A. Manzanares, S. Mafé, Ion size effects on the current efficiency of narrow charged pores, *J. Membr. Sci.* 191 (2001) 179187.
- [20] R. Qiao, N.R. Aluru, Ion concentrations and velocity profiles in nanochannel electroosmotic flows, *J. Chem. Phys.* 118 (2003) 4692–4701.
- [21] L. Joly, C. Ybert, E. Trizac, L. Bocquet, Hydrodynamics within the electric double layer on slipping surfaces, *Phys. Rev. Lett.* 93 (2004) 257805.
- [22] D. Antypov, M.C. Barbosa, C. Holm, Incorporation of excluded-volume correlations into Poisson–Boltzmann theory, *Phys. Rev. E* 71 (2005) 061106.
- [23] C.D. Santangelo, Computing counterion densities at intermediate coupling, *Phys. Rev. E* 73 (2006) 041512.
- [24] G. Tresset, Generalized Poisson–Fermi formalism for investigating size correlation effects with multiple ions, *Phys. Rev. E* 78 (2008) 061506.
- [25] Y. Liu, M. Liu, W.M. Lau, J. Yang, Ion size and image effect on electrokinetic flows, *Langmuir* 24 (2008) 2884–2891.
- [26] B. Eisenberg, Y. Hyon, C. Liu, Energy variational analysis EnVarA of ions in water and channels: field theory for primitive models of complex ionic fluids, *J. Chem. Phys.* 133 (2010) 104104.
- [27] J.J. Howard, J.S. Perkyus, B.M. Pettitt, The behavior of ions near a charged wall—dependence on ion size, concentration, and surface charge, *J. Phys. Chem. B* 114 (2010) 6074–6083.
- [28] S. Zhou, Z. Wang, B. Li, Mean-field description of ionic size effects with non-uniform ionic sizes: a numerical approach, *Phys. Rev. E* 84 (2011) 021901.
- [29] M.Z. Bazant, B.D. Storey, A.A. Kornyshev, Double layer in ionic liquids: overscreening versus crowding, *Phys. Rev. Lett.* 106 (2011) 046102.
- [30] G.-W. Wei, Q. Zheng, Z. Chen, K. Xia, Variational multiscale models for charge transport, *SIAM Rev.* 54 (2012) 699–754.
- [31] A. Warshel, S.T. Russell, Calculations of electrostatic interactions in biological systems and in solutions, *Q. Rev. Biophys.* 17 (1984) 283–422.
- [32] M.E. Davis, J.A. McCammon, Electrostatics in biomolecular structure and dynamics, *Chem. Rev.* 90 (1990) 509–521.
- [33] B. Honig, A. Nicholls, Classical electrostatics in biology and chemistry, *Science* 268 (1995) 1144–1149.
- [34] D. Andelman, Electrostatic properties of membranes: the Poisson–Boltzmann theory, in: R. Lipowsky, E. Sackmann (Eds.), *Handbook of Biological Physics*, 1, Elsevier, 1995, pp. 603–642.
- [35] P. Attard, Electrolytes and the electric double layer, *Adv. Chem. Phys.* 92 (1996) 1–159.
- [36] V. Vlachy, Ionic effects beyond Poisson–Boltzmann theory, *Ann. Rev. Phys. Chem.* 50 (1999) 145–165.
- [37] R.R. Netz, H. Orland, Beyond Poisson–Boltzmann: fluctuation effects and correlation functions, *Eur. Phys. J. E* 1 (2000) 203–214.
- [38] A.A. Kornyshev, Double-layer in ionic liquids: paradigm change?, *J. Phys. Chem. B* 111 (2007) 5545–5557.
- [39] P. Grochowski, J. Trylska, Continuum molecular electrostatics, salt effects and counterion binding – A review of the Poisson–Boltzmann model and its modifications, *Biopolymers* 89 (2008) 93–113.
- [40] M.Z. Bazant, M.S. Kilic, B.D. Storey, A. Ajdari, Towards an understanding of induced-charge electrokinetics at large applied voltages in concentrated solutions, *Adv. Coll. Interf. Sci.* 152 (2009) 48–88.
- [41] B. Eisenberg, Crowded charges in ion channels, *Advances in Chemical Physics*, John Wiley & Sons, Inc., 2011, pp. 77–223.
- [42] I. Borukhov, D. Andelman, H. Orland, Adsorption of large ions from an electrolyte solution: a modified Poisson–Boltzmann equation, *Electrochim. Acta* 46 (2000) 221–229.
- [43] J.W. Cahn, J.E. Hilliard, Free energy of a non-uniform system I. Interfacial free energy, *J. Chem. Phys.* 28 (1958) 258–267.
- [44] Y.K. Hyon, B. Eisenberg, C. Liu, A mathematical model for the hard sphere repulsion in ionic solutions, *Commun. Math. Sci.* 9 (2011) 459–475.
- [45] Y.K. Hyon, J.E. Fonseca, B. Eisenberg, C. Liu, Energy variational approach to study charge inversion (layering) near charged walls, *Discrete Contin. Dyn. Sys. Ser. A* 17 (2012) 2725–2743.
- [46] T.-L. Horng, T.-C. Lin, C. Liu, B. Eisenberg, PNP equations with steric effects: a model of ion flow through channels, *J. Chem. Phys. B* 116 (2012) 11422–11441.
- [47] G.-W. Wei, Differential geometry based multiscale models, *Bull. Math. Biol.* 72 (2010) 1562–1622.
- [48] M.F. Sanner, A.J. Olson, J.C. Spehner, Reduced surface: an efficient way to compute molecular surfaces, *Biopolymers* 38 (1996) 305–320.
- [49] D. Boda, M. Valiskó, B. Eisenberg, W. Nonner, D. Henderson, D. Gillespie, The effect of protein dielectric coefficient on the ionic selectivity of a calcium channel, *J. Chem. Phys.* 125 (2006) 034901.
- [50] L. Hu, G.-W. Wei, Nonlinear Poisson equation for heterogeneous media, *Biophys. J.* 103 (2012) 758–766.
- [51] L. Rayleigh, Some general theorems relating to vibrations, *Proc. London Math. Soc.* IV (1873) 357–368.
- [52] L. Onsager, Reciprocal relations in irreversible processes. I., *Phys. Rev.* 37 (1931) 405–426.
- [53] L. Onsager, Reciprocal relations in irreversible processes. II., *Phys. Rev.* 38 (1931) 2265–2279.
- [54] M.A. Biot, *Variational Principles in Heat Transfer: A Unified Lagrangian Analysis of Dissipative Phenomena*, Oxford University Press, New York, 1970.
- [55] F.-H. Lin, C. Liu, P. Zhang, On hydrodynamics of viscoelastic fluids, *Commun. Pure Appl. Math.* 58 (2005) 1437–1471.
- [56] W. Im, B. Roux, Ion permeation and selectivity of ompf porin: a theoretical study based on molecular dynamics, Brownian dynamics, and continuum electrodiffusion theory, *J. Mol. Biol.* 322 (2002) 851–869.
- [57] B. Corry, S. Kuyucak, S.-H. Chung, Dielectric self-energy in Poisson–Boltzmann and Poisson–Nernst–Planck models of ion channels, *Biophys. J.* 84 (2003) 3594–3606.
- [58] P. Graf, M.G. Kurnikova, R.D. Coalson, A. Nitzan, Comparison of dynamic lattice Monte Carlo simulations and the dielectric self-energy Poisson–Nernst–Planck continuum theory for model ion channels, *J. Phys. Chem. B* 108 (2004) 2006–2015.
- [59] O.P. Choudhary, R. Ujwal, W. Kowallis, R. Coalson, J. Abramson, M. Grabe, The electrostatics of VDAC: implications for selectivity and gating, *J. Mol. Biol.* 396 (2010) 580–592.
- [60] B. Nadler, U. Hollerbach, R.S. Eisenberg, Dielectric boundary force and its crucial role in gramicidin, *Phys. Rev. E* 68 (2003) 021905.
- [61] A. Mamonov, R.D. Coalson, A. Nitzan, M.G. Kurnikova, The role of the dielectric barrier in narrow biological channels: a novel composite approach to modeling single channel currents, *Biophys. J.* 84 (2003) 3646–3661.
- [62] B. Nadler, Z. Schuss, U. Hollerbach, R.S. Eisenberg, Saturation of conductance in single ion channels: the blocking effect of the near reaction field, *Phys. Rev. E* 70 (2004) 051912.
- [63] R.D. Coalson, M.G. Kurnikova, Poisson–Nernst–Planck theory approach to the calculation of current through biological ion channels, *IEEE Trans. Nanobiosci.* 4 (2005) 81–93.
- [64] M.H. Cheng, R.D. Coalson, An accurate and efficient empirical approach for calculating the dielectric self-energy and ion–ion pair potential in continuum models of biological ion channels, *J. Phys. Chem. B* 4 (2005) 81–93.
- [65] A. Duncan, R.D. Sedgewick, R.D. Coalson, Improved local lattice approach for Coulombic simulations, *Phys. Rev. E* 71 (2005) 046702.
- [66] D. Boda, W. Nonner, M. Valiskó, D. Henderson, B. Eisenberg, D. Gillespie, Steric selectivity in Na channels arising from protein polarization and mobile side chains, *Biophys. J.* 93 (2007) 1960–1980.
- [67] D. Boda, M. Valiskó, B. Eisenberg, W. Nonner, D. Henderson, D. Gillespie, The combined effect of pore radius and protein dielectric coefficient on the selectivity of a calcium channel, *Phys. Rev. Lett.* 98 (2007) 168102.

- [68] D. Boda, D. Henderson, B. Eisenberg, D. Gillespie, A method for treating the passage of a charged hard sphere ion as it passes through a sharp dielectric boundary, *J. Chem. Phys.* 135 (2011) 064105.
- [69] B. Li, X. Cheng, Z. Zhang, Dielectric boundary force in molecular solvation with the Poisson–Boltzmann free energy: a shape derivative approach, *SIAM J. Appl. Math.* 71 (2011) 2093–2111.
- [70] N.A. Simakov, M.G. Kurnikova, Soft wall ion channel in continuum representation with application to modeling ion currents in α -Hemolysin, *J. Phys. Chem. B* 114 (2010) 15180–15190.
- [71] Y. Mori, C. Liu, R.S. Eisenberg, A model of electrodiffusion and osmotic water flow and its energetic structure, *Biophys. J.* 100 (2011) 86a–87a.
- [72] B. Eisenberg, Multiple scales in the simulation of ion channels and proteins, *J. Phys. Chem. C* 114 (2010) 20719–20733.
- [73] B. Eisenberg, A leading role for mathematics in the study of ionic solutions, *SIAM News* 45 (2012) 11–12.
- [74] B. Eisenberg, Ionic interactions are everywhere, *Physiology (Bethesda)* 28 (2013) 28–38.
- [75] W. Geng, S. Yu, G. Wei, Treatment of charge singularities in implicit solvent models, *J. Chem. Phys.* 127 (2007) 114106.
- [76] B. Lu, J.A. McCammon, Molecular surface-free continuum model for electrodiffusion processes, *Chem. Phys. Lett.* 451 (2008) 282–286.
- [77] A. Shrake, J.A. Rupley, Environment and exposure to solvent of protein atoms, Lysozyme and insulin, *J. Mol. Biol.* 79 (1973) 351–371.
- [78] B.Z. Lu, Y.C. Zhou, M.J. Holst, J.A. McCammon, Recent progress in numerical methods for the Poisson–Boltzmann equation in biophysical applications, *Commun. Comput. Phys.* 3 (2008) 973–1009.
- [79] Q. Zheng, D. Chen, G.-W. Wei, Second-order Poisson Nernst–Planck solver for ion channel transport, *J. Comput. Phys.* 230 (2011) 5239–5262.
- [80] J. Ortega, W.C. Rheinboldt, *Iterative Solutions of Nonlinear Equations in Several Variables*, Academic Press, New York, 1970.
- [81] D. Boda, W.R. Fawcett, D. Henderson, S. Sokolowski, Monte Carlo, density functional theory, and Poisson–Boltzmann theory study of the structure of an electrolyte near an electrode, *J. Chem. Phys.* 116 (2002) 7170.
- [82] A. Malasics, D. Gillespie, W. Nonner, D. Henderson, B. Eisenberg, D. Boda, Protein structure and ionic selectivity in calcium channels: Selectivity filter size, not shape, matters, *Biochim. Biophys. Acta* 1788 (2009) 2471–2480.
- [83] I.-L. Chern, J.-G. Liu, W.-C. Wang, Accurate evaluation of electrostatics for macromolecules in solution, *Meth. Appl. Anal.* 10 (2003) 309–328.
- [84] S.M. Hou, X.-D. Liu, A numerical method for solving variable coefficient elliptic equation with interfaces, *J. Comput. Phys.* 202 (2005) 411–445.
- [85] W. Humphrey, A. Dalke, K. Schulten, VMD - Visual Molecular Dynamics, *J. Mol. Graphics* 14 (1996) 33–38.
- [86] J.-L. Liu, W.C. Rheinboldt, A posteriori finite element error estimators for parametrized nonlinear boundary value problems, *Numer. Funct. Anal. Opt.* 17 (1996) 605–637.
- [87] C. Tanford, *Physical Chemistry of Macromolecules*, John Wiley & Sons, New York, 1961.
- [88] J.W. Jerome, Consistency of semiconductor modeling: an existence/stability analysis for the stationary van roosbroeck system, *SIAM J. Appl. Math.* 45 (1985) 565–590.
- [89] R.S. Varga, *Matrix Iterative Analysis*, Prentice-Hall, Englewood Cliffs, NJ, 1962.
- [90] R.E. Bank, D.J. Rose, Some error estimates for the box method, *SIAM J. Numer. Anal.* 24 (1987) 777–787.
- [91] J.-L. Liu, On weak residual error estimation, *SIAM J. Sci. Comput.* (1996) 1249–1268.
- [92] A. Brandt, Multi-level adaptive solutions to boundary-value problems, *Math. Comput.* 31 (1977) 333–390.
- [93] R.S. Dembo, S.C. Eisenstat, T. Steihaug, Inexact Newton methods, *SIAM J. Numer. Anal.* 19 (1982) 400–408.
- [94] M. Holst, F. Saied, Numerical solution of the nonlinear Poisson–Boltzmann equation: developing more robust and efficient methods, *J. Comput. Chem.* 16 (1995) 337–364.
- [95] R.-C. Chen, J.-L. Liu, An accelerated monotone iterative method for the quantum-corrected energy transport model, *J. Comput. Phys.* 227 (2008) 6240–6266.
- [96] H.M. Berman et al, The protein data bank, *Acta Cryst.* D58 (2002) 899–907.
- [97] R.R. Ketchum, K.C. Lee, S. Huo, T.A. Cross, Macromolecular structural elucidation with solid-state NMR-derived orientational constraints, *J. Biomol. NMR* 8 (1996) 1–14.
- [98] T.J. Dolinsky, P. Czodrowski, H. Li, J.E. Nielsen, J.H. Jensen, G. Klebe, N.A. Baker, PDB2PQR: expanding and upgrading automated preparation of biomolecular structures for molecular simulations, *Nucl. Acids Res.* 35 (2007) W522–W525.
- [99] W. Im, D. Beglov, B. Roux, Continuum solvation model: computation of electrostatic forces from numerical solutions to the Poisson–Boltzmann equation, *Comput. Phys. Commun.* 111 (1998) 59–75.
- [100] M. Holst, N. Baker, F. Wang, Adaptive multilevel finite element solution of the Poisson–Boltzmann equation I. Algorithms and examples, *J. Comput. Chem.* 21 (2000) 1319–1342.